Biophysics Reports

CrossMark

Perilipin 2 and lipid droplets provide reciprocal stabilization

Shimeng Xu[1,2], **Fei Zou**[3,4], **Zhiqing Diao**[5,6], **Shuyan Zhang**[1], **Yaqin Deng**[1],
Xiaotong Zhu[1,2], **Liujuan Cui**[1,7], **Jinhai Yu**[1,2], **Zhiguang Zhang**[8],
Adekunle Toyin Bamigbade[1], **Hongchao Zhang**[4], **Xuan Wei**[4], **Xuelin Zhang**[9],
Bin Liang[6✉], **Pingsheng Liu**[1✉]

[1] National Laboratory of Biomacromolecules, CAS Center for Excellence in Biomacromolecules, Institute of Biophysics, Chinese Academy of Sciences, Beijing 100101, China
[2] University of Chinese Academy of Sciences, Beijing 100049, China
[3] Graduate School of Anhui Medical University, Hefei 230032, China
[4] General Hospital of Air Force, Beijing 100142, China
[5] School of Life Sciences, Anhui University, Hefei 230601, China
[6] Key Laboratory of Animal Models and Human Disease Mechanisms of Chinese Academy of Science & Yunnan Province, Kunming Institute of Zoology, Chinese Academy of Sciences, Kunming 650223, China
[7] School of Life Sciences, University of Science and Technology of China, Hefei 230032, China
[8] Department of Cell Biology and Genetics, School of Basic Medical Sciences, Fujian Medical University, Fuzhou 350004, China
[9] School of Kinesiology and Health, Capital University of Physical Education and Sports, Beijing 100191, China

Abstract The lipid droplet (LD)-associated protein adipose differentiation-related protein (ADRP or PLIN2) is required for the formation and stability of the LD organelle, whereas its biological roles are still obscure. Herein, we show that PLIN2 is the most abundant protein on the lipid droplets (LDs) of mouse myoblast cell line C2C12. Both the expression of PLIN2 and the accumulation of LDs were up-regulated in a time- and dose-dependent manner when the cells were treated with oleate (OA). The protein level of PLIN2 was positively correlated with the formation of LDs, suggesting that LDs stabilize PLIN2. Furthermore, knocking out PLIN2 in C2C12 cells led to enlarged LDs and higher triacylglycerol hydrolysis activity. The isolated PLIN2 null LDs became closely contact with mitochondria and other cellular organelles. Additionally, mitochondrial activity was suppressed by OA in PLIN2 null cells. Our results reveal the pivotal roles of PLIN2 in governing LD dynamics and their relationship to mitochondria, and suggest a reciprocal stabilization between PLIN2 and LDs.

Keywords Lipid droplets, PLIN2, Triacylglycerol, Mitochondria, Hydrolysis

Shimeng Xu, Fei Zou and Zhiqing Diao have contributed equally to this work.

✉ Correspondence: liangb@mail.kiz.ac.cn (B. Liang), pliu@ibp.ac.cn (P. Liu)

INTRODUCTION

Obesity develops when energy intake exceeds energy expenditure, leading to lipid accumulation in adipose tissues and nonadipose tissues (*e.g.,* liver, muscle, *etc.*), which alters systemic metabolism and can lead to metabolic syndrome (Murphy *et al.* 2009; Unger *et al.*

2010). Lipid droplets (LDs) are highly dynamic organelles that are composed primarily of triacylglycerol (TAG) and sterol esters (SE), which form a neutral lipid core, and are wrapped by a monolayer of phospholipids with numerous resident proteins (Brown 2001). LDs serve as the primary mobile cellular reservoir for lipid-based energy and membrane precursors (Fujimoto and Parton 2011). The dynamic of LDs has been considered as an important indicator for the metabolic states of cells and tissues (Greenberg et al. 2011). For example, excessive lipid accumulation in LDs can lead to obesity, fatty liver, diabetes, and atherosclerosis. Similarly, a lack of lipid or LDs can lead to diseases such as neutral lipid storage disease and lipodystrophy.

Perilipin1 (PLIN1), adipocyte differentiation-related protein (ADRP/PLIN2), Tip47 (PLIN3), S3-12 (PLIN4), and OXPAT (PLIN5), also collectively called "PAT" family proteins, were recently renamed the Perilipins (PLIN) 1–5 (Kimmel et al. 2010) and are the main structural proteins of LDs (Bickel et al. 2009; Brasaemle 2007; Greenberg et al. 2011; Walther and Farese 2012). Of which, PLIN2 is ubiquitously expressed as a lipid droplet (LD)-associated protein (Brasaemle et al. 1997), and has been shown to play a key role in LD formation (Fukushima et al. 2005) and maintenance of lipid homeostasis. PLIN2 is thought to be involved in both LD biogenesis and the regulation of lipolysis, primarily in adipocytes, but also in other cells and tissues (Chang et al. 2006; Listenberger et al. 2007; Robenek et al. 2006). PLIN2 null mice display reduced hepatic lipids, and are resistant to diet-induced fatty liver without detectable changes in TAG synthesis, or fatty acid uptake, synthesis, or β-oxidation (Chang et al. 2006; McManaman et al. 2013). Furthermore, PLIN2 null *ob/ob* mice (*leptin*$^{-/-}$) show improved insulin sensitivity and reduced hepatosteatosis compared to controls that are only leptin-deficient (Chang et al. 2010). Additionally, *in vitro* results reveal that overexpression of PLIN2 increases both TAG accumulation and LD formation (Fukushima et al. 2005; Larigauderie et al. 2006; Listenberger et al. 2007), which may be as the result of the reduced LD localization of adipose triglyceride lipase (ATGL) and the slowdown of TAG turnover (Listenberger et al. 2007). Conversely, knockdown of PLIN2 in macrophages is shown to decrease cellular lipids and LD size and number (Larigauderie et al. 2006). These results demonstrate an important role of PLIN2 in the regulation of LD dynamic and TAG metabolism.

Skeletal muscle is a crucial metabolic organ which plays an important role in energy expenditure. The overall amount of TAG in skeletal muscle is quite small compared to that in adipose tissue, but an increase in skeletal muscle TAG is a major contributor to insulin resistance (Kelley et al. 1999; Pan et al. 1997). In skeletal muscle, PLIN2 is the most abundantly expressed PLIN protein (Brasaemle et al. 1997; Heid et al. 1998; MacPherson and Peters 2015b; Minnaard et al. 2009; Peters et al. 2012). PLIN2 overexpression either *in vitro* or *in vivo* increases intramyocellular LD accumulation and TAG storage, and also improves skeletal muscle insulin sensitivity, whereas PLIN2 knockdown displays opposite effects (Bosma et al. 2012). However, the exact relationship between PLIN2 expression and TAG accumulation is still unclear (MacPherson and Peters 2015a). In addition, PLIN2 distribution and association with LDs remain ambiguous. For example, PLIN2 was reported to highly co-localize to the LD surface in isolated rat soleus fibers (Prats et al. 2006), whereas other studies have found contradictory results in isolated rat soleus muscle (MacPherson et al. 2012) and human vastus lateralis (Shaw et al. 2009).

Thus, to explore the role of PLIN2 in skeletal muscle, we isolated LDs from the mouse myoblast cell line C2C12. We found that PLIN2 was the most abundant protein on the LDs, and its expression was up-regulated in a time- and dose-dependent manner in the presence of oleate (OA). The accumulation of TAG and the formation of LDs may promote the stability of the PLIN2 protein. Knock out (KO) of PLIN2 in C2C12 cells led to larger LDs that were fewer in number under both basal and OA treatment, and also resulted in higher hydrolysis activity during OA treatment, compared to wild type (WT) cells. The KO of PLIN2 increased the contact between LDs and mitochondria, and inhibited mitochondrial activity during OA treatment.

RESULTS

Oleate (OA) upregulates PLIN2 expression and lipid droplet (LD) expansion

Excessive accumulation of lipids in LDs has been linked to many metabolic disorders. The roles of ubiquitously-expressed LD structure protein PLIN2 in the lipid accumulation of LDs remains elusive. To do so, we cultured C2C12 myoblasts in the presence or absence of OA to induce a model of lipid overload. From these cells LDs were isolated and biochemical measurements were made to determine the purity of isolated LDs. First, we compared the protein profile of isolated LDs to other cell fractions using silver staining. Proteins extracted from LDs displayed a relatively simple pattern that was obviously distinct from the protein profiles of the other three cellular fractions, including post-nuclear supernatant (PNS), total membranes (TM), and cytosol (Cyto)

(Fig. 1A). The purity of isolated LDs was further assessed by the relative enrichment of LD-associated proteins PLIN2 and PLIN3, and the absence of markers that correspond to other intracellular compartments, lysosome protein Lamp1, ER protein Bip, mitochondrion protein Tim23, and cytoplasmic protein GAPDH. As previously reported (Liu *et al*. 2004), the plasma membrane protein Cav-1 was also found in the LD fraction, and its expression was induced by OA treatment (Fig. 1A). Collectively, these results suggest that the isolated LD fraction from C2C12 cells might be largely free of contamination.

OA treatment increased the expression of the most abundant band in the LD fraction (Fig. 1A). ImageJ analysis showed that the density of this band occupied about 25% and 41% of total LD proteins in the absence or presence of OA, respectively (Fig. 1B). Therefore, this band was sliced and then subjected to mass spectrometry (MS) analysis. Its major protein was identified as PLIN2 (supplementary material Table S1). Consistent with the MS results, immunoblot results also confirmed that the expression of PLIN2 was increased in the LD fraction with OA treatment (Fig. 1A).

To investigate the relationship between the expression of PLIN2 and the formation of LDs, we treated mouse C2C12 myoblasts with 200 μmol/L OA for the indicated times or with different concentrations of OA for 12 h (Fig. 1C, D). The mRNA and the protein levels of PLIN2 were up-regulated by OA treatment in a dose- and time-dependent manner (Fig. 1C, D). The protein level of PLIN2 increased much more dramatically than its mRNA level, implying that OA may enhance the stability of the PLIN2 protein. In addition, PLIN2–EGFP knock-in (KI) C2C12 cells also showed that the intensity of GFP fluorescence was enhanced in a time- and dose-dependent manner under OA incubation (Fig. 1E, F, supplementary material Fig. S1B). Similarly, TAG content was significantly increased by OA incubation in a time-dependent manner (Fig. 1G). OA treatment also dramatically increased LD number and size, concomitant with the accumulation of TAG (Fig. 1H). Therefore, these results demonstrate that both PLIN2 and LDs are up-regulated by OA.

Disruption of lipid droplets (LDs) reduces the stability of PLIN2

Since the expression of PLIN2 is positively related to TAG accumulation and LD formation during OA treatment, we asked whether PLIN2 expression promotes TAG accumulation and LD formation; or, conversely, whether TAG accumulation and LD formation induce PLIN2 expression and stabilization. To answer this

question, we constructed cell models that contained reduced TAG and LDs to detect the level of PLIN2 expression during the incubation with OA. Diacylglycerol acyltransferase 1 and 2 (DGAT1/2) are the key enzymes in the final, committed step of TAG biosynthesis (Yen *et al*. 2008). ATGL plays a key role in the hydrolysis of TAG (Villena *et al*. 2004; Zimmermann *et al*. 2004, 2009). We therefore constructed *Atgl* over-expressed (OE) and *Dgat1/Dgat2* double knock-out (DKO) C2C12 cell lines (Fig. 2D, supplementary material Fig. S2) to reduce the accumulation of TAG and LDs during incubation with OA.

The *Dgat1/Dgat2* DKO cells accumulated much less TAG and formed much fewer LDs during OA treatment (Fig. 2A, B). Interestingly, we found that the mRNA level of PLIN2 was induced during OA incubation in the *Dgat1/Dgat2* DKO cells to a degree similar to WT cells (Fig. 2C), whereas the protein expression level of PLIN2 was not induced in *Dgat1/Dgat2* DKO cells (Fig. 2D). Therefore, it appears that accumulation of LDs is required to stabilize the PLIN2 protein and thus LDs perform a crucial role in protecting PLIN2 from rapid degradation.

We then treated C2C12 cells with palmitate (PA) and/ or OA, and measured the expression and accumulation of PLIN2 and LDs to verify this finding (Coll *et al*. 2008; Gao *et al*. 2009; Peng *et al*. 2011; Salvado *et al*. 2013). PA and PA plus OA dramatically induced PLIN2 mRNA expression even greater than OA (Fig. 2E). However, PA treatment did not increase the level of PLIN2 protein, unlike treatment with OA or PA plus OA (Fig. 2G).

PA induced the formation of many fewer LDs than OA or PA plus OA, as expected (Fig. 2F). In addition, the expression level of exogenous PLIN2-MYC protein was much lower in PA-treated cells than in the cells that were incubated with OA and PA plus OA (Fig. 2G). Since the transcriptional levels of exogenous PLIN2-MYC could not be stimulated by free fatty acid, the higher expression level of its protein represents an increase in stability of the protein in OA- or PA plus OA-treated cells (Fig. 2F, G). The results further strengthen the conclusion that LDs enhance the stability of PLIN2.

Depletion of PLIN2 enhances lipid droplet size and lipolysis

The results described indicate that OA stimulated both PLIN2 expression and LD formation and that the formation of LDs stabilized the newly manufactured PLIN2. We then asked whether PLIN2 affects the formation and dynamics of LDs since it is the most abundant protein on LDs of C2C12 cells. To do so, PLIN2 KO C2C12 cells were generated. Previous work showed that methionine
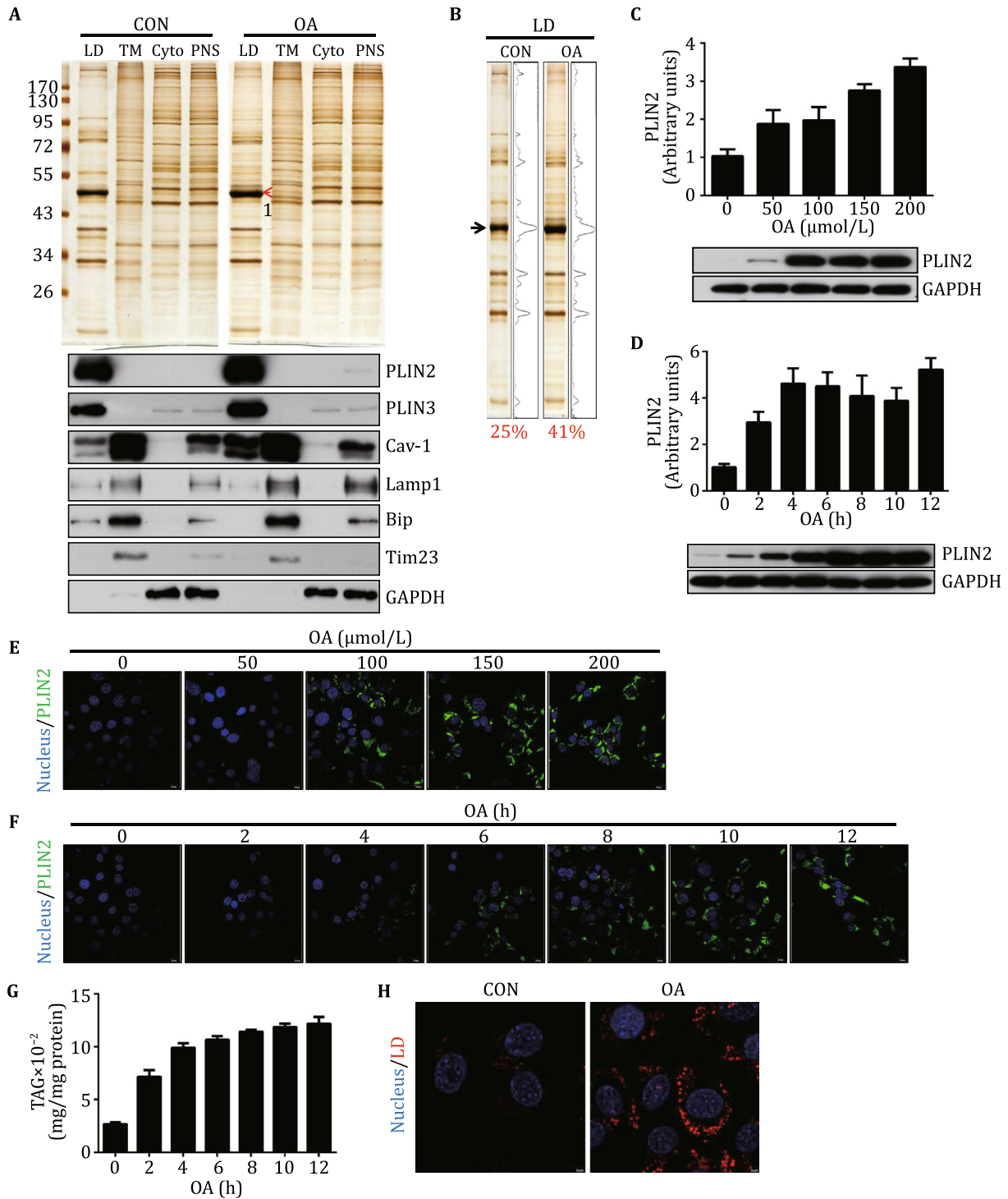
Fig. 1 Both PLIN2 and LDs are up-regulated by free fatty acids. **A** Silver staining and Western blot analysis of proteins from LDs and other fractions of C2C12 cells after treatment with or without OA. The band indicated by the *red arrow* was sliced for MS analysis. Marker proteins of cellular components were used to verify the purity of LDs (PLIN2/3: LDs, Cav-1: plasma membrane, Lamp1: lysosome, Bip: ER, Tim23: mitochondria, GAPDH: cytosol). **B** Quantification of silver stained LD proteins by ImageJ. **C, D** The mRNA and the protein levels of PLIN2 in C2C12 cells after treatment with OA at the indicated concentrations (**C**) or times (**D**). These results had at least three biological repeats. **E, F** EGFP fluorescence intensity of PLIN2-EGFP KI C2C12 cells after treatment with OA at the indicated concentrations (**E**) or time (**F**). Scale bar, 20 μm. **G** The TAG content (TAG/protein) in C2C12 cells after treatment with OA for the indicated times. Data were collected from two biological repeats. **H** LD fluorescence intensity in C2C12 cells after treatment with OA. LDs were stained with LTR and imaged with a confocal microscope. Scale bar, 5 μm
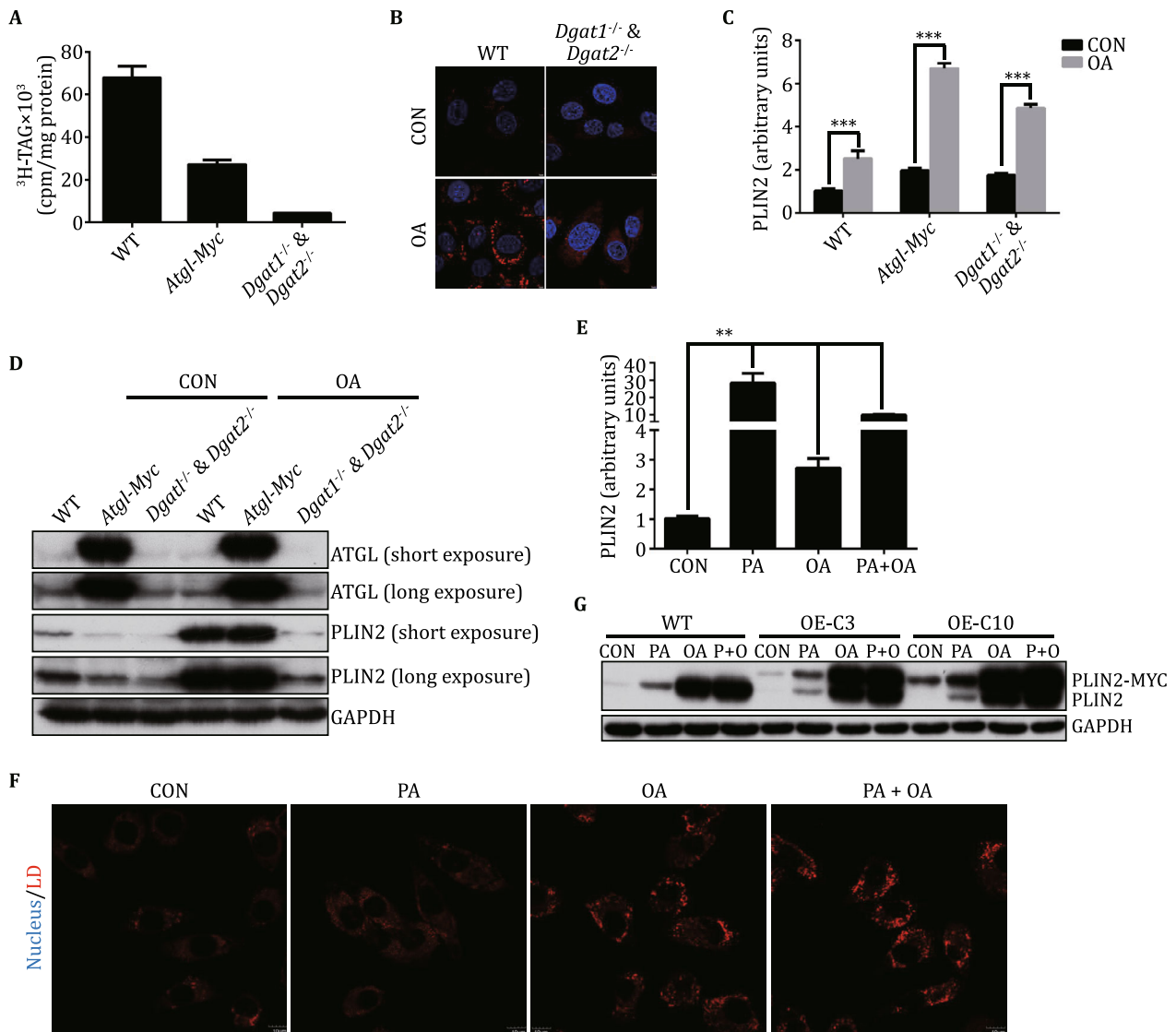
Fig. 2 Disruption of LDs reduces the stability of PLIN2. **A** TAG content (TAG/protein) of WT, *Atgl* overexpressed, and *Dgat1*/*Dgat2* DKO C2C12 cells after treatment with OA and 0.5 μCi/mL ^{3}H-OA for 6 h. **B** LD fluorescence intensity of WT and *Dgat1*/*Dgat2* DKO C2C12 cells after treatment with or without OA for 12 h. LDs were stained with LTR and were imaged by confocal microscope. Scale bar, 5 μm. **C, D** The mRNA (**C**) and protein (**D**) levels of PLIN2 in WT, *Atgl* overexpressed, and *Dgat1*/*Dgat2* DKO C2C12 cells after treatment with or without OA for 6 h. Data were collected from two biological repeats. **E, F** The mRNA level of PLIN2 (**E**) and the LD fluorescence intensity (**F**) of C2C12 cells after treatment with PA and/or OA. LDs were stained with LTR and were imaged with a confocal microscope. Scale bar, 10 μm. The results from **E** had at least three biological repeats. **G** The protein expression level of endogenous PLIN2 and exogenous PLIN2-MYC of C2C12 cells after treatment with PA and/or OA. All the data presented as mean ± SEM. Significant difference between two groups, **$p < 0.01$, ***$p < 0.001$

123 of the PLIN2 coding sequence might represent an initiation site of a short isoform of mouse PLIN2 (Russell *et al.* 2008). Thus, we designed two targets to knock out PLIN2, with one between amino acids (aa) 166–172 and the other between aa 79–86. Finally, two clones, T1C13 (PLIN2 KO Target1 clone13) and T2C9 (PLIN2 KO Target2 clone9), were isolated for further study (Fig. 3A, B).

We measured the accumulation of TAG in the PLIN2 KO cells since TAG is the major neutral lipid stored in

LDs of C2C12 cells (data not shown). We treated WT and T1C13 cells with or without OA for 12 h. There was no significant difference in TAG content between untreated WT and PLIN2 KO cells (Fig. 3C). However, when treated with OA, T1C13 cells accumulated significantly less TAG compared to WT cells (Fig. 3C).

Next, we asked whether the reduced TAG accumulation in PLIN2 KO cells was due to an imbalance between TAG synthesis and lipolysis. The empty vector-transfected (EV) and PLIN2 KO C2C12 cells were treated with
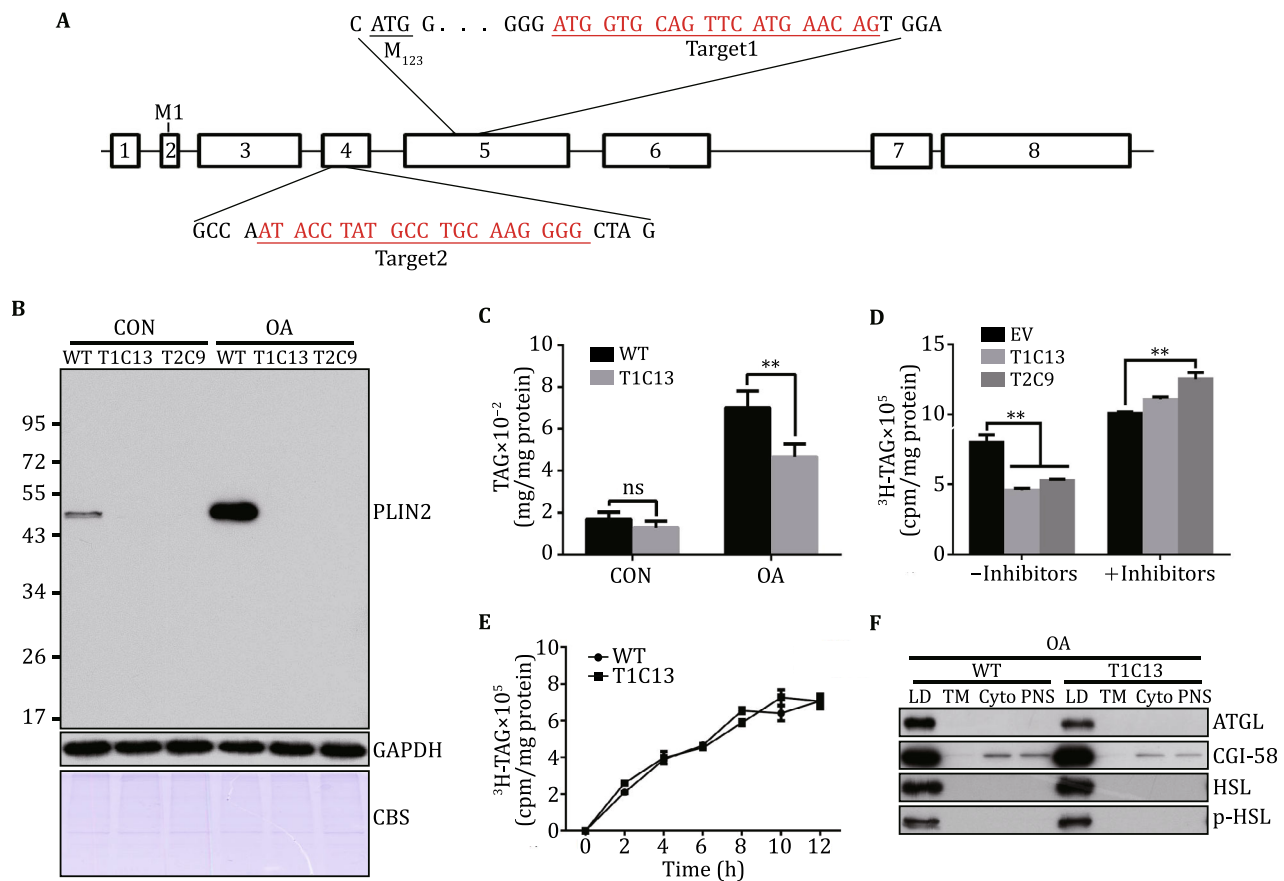
Fig. 3 Depletion of PLIN2 enhances LD lipolysis. **A** The diagram of the two targets used in the PLIN2 genomic KO. The gRNAs of PLIN2 was targeted to Exon5 (Target1) and Exon4 (Target2) respectively. **B** Western blot of PLIN2 to verify the KO of PLIN2 in C2C12 cells. **C** TAG accumulation (TAG/protein) of WT and PLIN2 KO C2C12 cells after treatment with or without OA for 12 h. **D** EV and PLIN2 KO C2C12 were treated with OA, 0.5 μCi/mL ^{3}H-OA with or without lipase inhibitors for 12 h. After treatment the tritium was counted. **E** WT and T1C13 cells were treated with OA, 0.5 μCi/mL ^{3}H-OA and lipase inhibitors. TAG was extracted at the indicated times and the ^{3}H-TAG was counted. **F** Western blot analysis of isolated LD proteins (TAG lipolysis enzymes) from WT and T1C13 cells after treatment with OA. Data presented as mean ± SEM. Significant difference between two groups, **$p < 0.01$. The results from **C**, **D** and **E** had at least three biological repeats

or without lipase inhibitors (Atglistatin for the inhibition of ATGL, CAY10499 for the inhibition of HSL), along with OA plus a trace amount of ^{3}H-OA for 12 h. The EV cells accumulated more TAG than PLIN2 null cells without lipases inhibitors (Fig. 3D). However, both clones of PLIN2 KO cells (T1C13 and T2C9) accumulated slightly more TAG than EV cells in the presence of lipases inhibitors (Fig. 3D).

Consistently, the expression of both HSL and phosphorylated HSL was increased in the LD fraction of PLIN2 KO cells over that of WT cells while the expression of ATGL was slightly reduced (Fig. 3F). The purity of the LD fractions from WT and T1C13 cells was analyzed and the results shown in supplementary material Fig. S3. The LD fractions were significantly different from the other cellular fractions by silver staining, and

LD marker proteins PLIN2 and PLIN3 were highly enriched in the LD fractions (Fig. S3 Lanes 1 and 5).

When the cells were treated with lipases inhibitors and OA plus trace amount ^{3}H-OA for the indicated times, the WT and T1C13 cells showed no significant differences in the incorporation rate of ^{3}H-OA (Fig. 3E). Taken together, these lines of evidence suggest that PLIN2 probably increases TAG accumulation during OA incubation in C2C12 cells by preventing TAG hydrolysis, rather than by promoting TAG synthesis.

Upon determining that PLIN2 was important for the storage of TAG, we tested if PLIN2 would influence the morphology of LDs. To do so, the WT and PLIN2 KO cells were treated with or without OA for 12 h, and were then stained with LipidTox Red (LTR) for LDs and Hoechst for the nucleus. Compared with WT cells,

T1C13 and T2C9 cells showed fewer but larger LDs either with or without OA treatment (Fig. 4A). This visual impression was confirmed by quantification of size (Fig. 4B) and number (Fig. 4C). Thus, PLIN2 plays an important role in maintaining LD morphology.

Next, LDs from WT and T1C13 cells were isolated to study the differences between them at a subcellular level. Consistent with the cellular level study, the isolated LDs of T1C13 cells were larger than those from WT cells by morphological (Fig. 4D) and granulometric measures (Fig. 4E). The purity of the isolated LDs was determined as previously described (supplementary material Fig. S3). As visualized through silver staining, proteins extracted from LDs from T1C13 cells displayed more proteins than LDs from WT cells (supplementary material Fig. S3). A prominent band was conspicuously absent in the LD proteins from T1C13 cells (supplementary material Fig. S3 Lane 5 Band 2), confirming the identity of this band as PLIN2 in C2C12 LDs (Fig. 1A, B). In addition, a new band of approximately 55 kDa was detected in the proteins from the KO cell LDs (supplementary material Fig. S3, Lane 5 Band 1), which was identified as PLIN3 by proteomic analysis (supplementary material Table S2).

LDs isolated from PLIN2 KO cells were larger than those from WT cells (Fig. 4D, E), which may be due to the compensatory expression of PLIN3 on LDs. To test this possibility, PLIN3 was knocked out in T1C13 cells, and then the LDs of these DKO cells were isolated and examined (supplementary material Fig. S4A and B). The size of LDs isolated from the DKO cells was larger than

those from the EV cells (supplementary material Fig. S4C), suggesting that the compensatory expression of PLIN3 on PLIN2 null LDs was not the reason for the enlarged LDs in the PLIN2 KO cells. Together, these data indicate that PLIN2, the protein stability of which is dependent on the formation of LDs, maintains certain LD size and number and protects TAG from lipolysis in return.

PLIN2 null lipid droplets (LDs) closely contact with mitochondria

LDs have been reported to contact other intracellular organelles including the endoplasmic reticulum (ER) (Ozeki *et al.* 2005), mitochondria (Pu *et al.* 2011), peroxisomes (Binns *et al.* 2006; Schrader 2001) and endosomes (Liu *et al.* 2007). As the most abundant protein on the LDs of C2C12 cells, PLIN2 may be involved in mediating these interactions. To investigate this possibility, LDs isolated from WT and T1C13 cells (supplementary material Fig. S3) were probed for the marker proteins of the other intracellular organelles by Western blot (Fig. 5). The levels of mitochondrial (Cpt1a, Cpt1b, Acsl1, Opa1, and Mfn1), ER (PDI and BIP), plasma membrane (Cav-1), and lysosomal (Lamp1) proteins were markedly increased in the LD fractions from T1C13 cells compared with those from WT cells (Fig. 5A).

Among all the proteins analyzed, the mitochondrial proteins were most dramatically increased (Fig. 5A), even though there were no significant differences in the cellular expression levels between WT and T1C13 cells
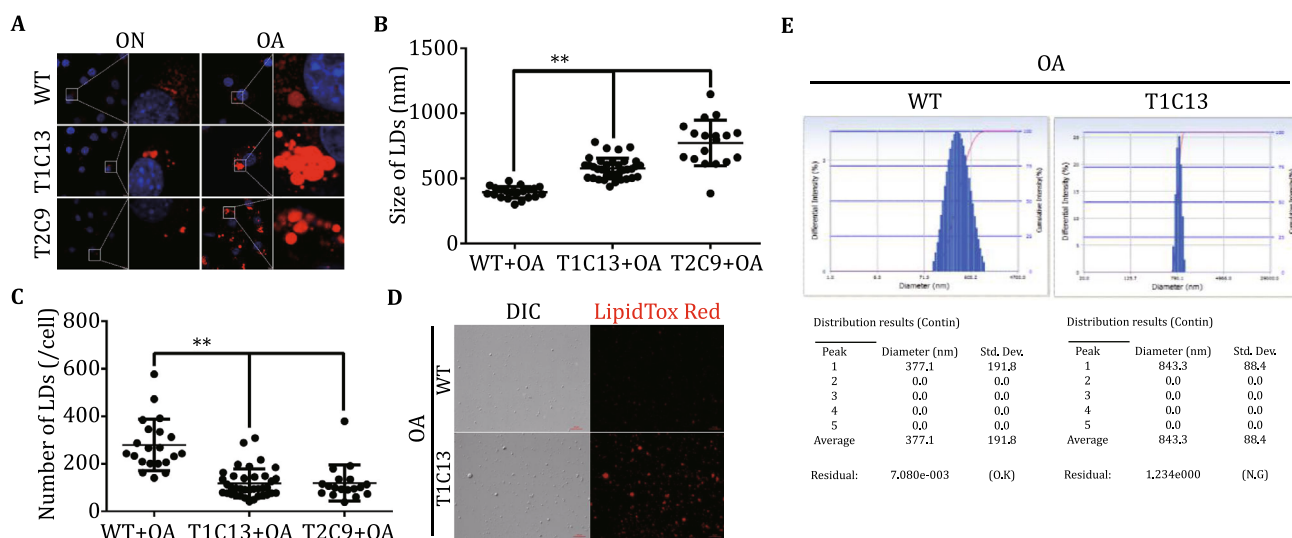

Fig. 4 Depletion of PLIN2 enhances LD size. **A** Confocal images of WT and PLIN2 KO cells stained with Hoechst and LTR. Scale bar, 10 μm. **B, C** Quantification of LDs size (**B**) and number (**C**) from confocal images analyzed by ImageJ. $N \geq 18$. These two data were reproducible from two biological repeats. **D, E** LDs of WT and T1C13 cells isolated after OA treatment. LTR staining of isolated LDs visualized using the Zeiss AxioImager M2 Imaging System, scale bar, 20 μm (**D**). The size of the isolated LDs was measured by a Delsa Nano C particle analyzer (**E**). Data presented as mean ± SEM. Significant difference between two groups, **$p < 0.01$
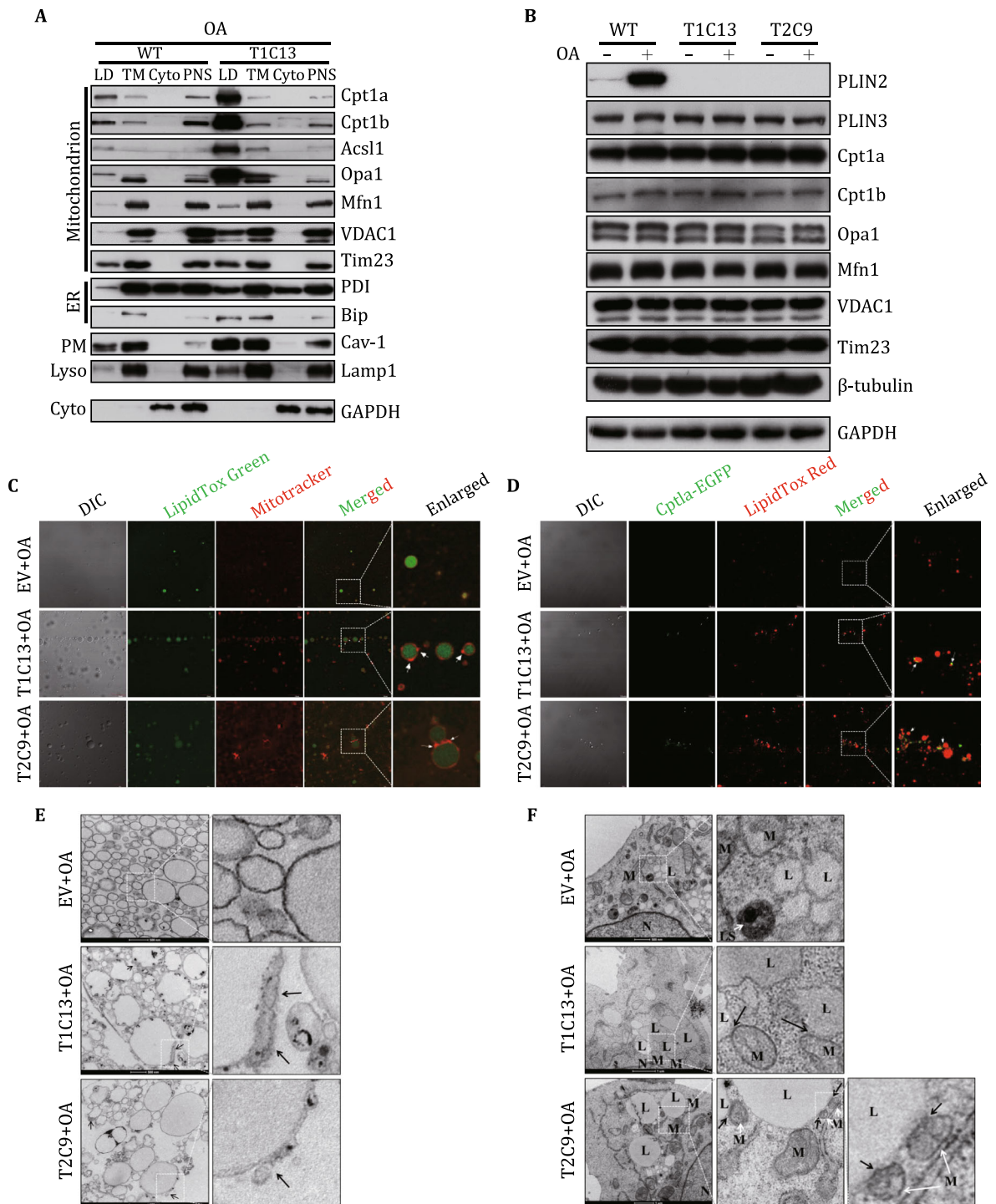
Fig. 5 PLIN2 null LDs closely contact with mitochondria. **A** Western blot analysis of LDs isolated from WT and T1C13 cells after treatment with OA. Cpt1a, Cpt1b, Acsl1, Opa1, Mfn1, VADC1, and Tim23 were markers for mitochondria; PDI and Bip were for ER; Cav-1 was for plasma membrane; Lamp1 was for lysosome; GAPDH was for cytosol. **B** Western blot analysis of whole cell lysates of WT and PLIN2 KO cells after treatment with or without OA. **C** Confocal microscopy of LDs isolated from OA-treated EV and PLIN2 KO C2C12 cells. LTG for LDs and MR for mitochondria. *White arrows* indicate the close connection between LD and mitochondrion. Scale bar, 10 μm. **D** Confocal microscopy of LDs isolated from OA-treated EV and PLIN2 KO C2C12 cells. All cell types were transfected with Cpt1a-EGFP before OA treatment. *White arrows* indicate the close connection between LD and Cpt1a-EGFP. Scale bar, 10 μm. **E** EM of the ultrastructure of isolated LDs with or without PLIN2. *Black arrows* indicate LD connected to mitochondria. Scale bar, 0.5 μm. **F** EM of the ultrastructure of LDs in EV and PLIN2 KO C2C12 cells. *Black arrows* indicate the interaction sites between LDs and mitochondria. *White arrows* indicate LD connected to mitochondria. Scale bar, 0.5 μm and 1 μm. M: mitochondrion; L: LD; N: nucleus; LS: lysosome

(Fig. 5B). This raised the question whether deletion of PLIN2 led to closer contact between LDs and mitochondria; or, alternatively, the re-localization of mitochondrial proteins to LDs. To address this question, LDs were isolated from OA-treated EV and PLIN2 KO cells (T1C13 and T2C9 clones) and were then double stained with LipidTox Green (LTG) and Mitotracker Red (MR). PLIN2 null LDs indeed showed more highly abundant punctate red signals on their surface than LDs from EV cells, suggesting an increased interaction between PLIN2 null LDs and mitochondria (Fig. 5C). Furthermore, LDs from OA-treated Cpt1a-EGFP-transfected EV and PLIN2 KO cells (supplementary material Fig. S5) were isolated and stained with LTR. In agreement with the findings with MR, PLIN2 null LDs showed much more connected green signal on their surface than that of EV cells (Fig. 5D). The cellular expression level of Cpt1a-EGFP in the EV cells and PLIN2 KO cells did not differ significantly (supplementary material Fig. S5). Moreover, transmission electron microscope (TEM) images showed that PLIN2 null LDs closely interacted with mitochondria as indicated by black arrows (Fig. 5E, F). Collectively, these results suggest that PLIN2 is a key player in the regulation of interactions between LDs and the other intracellular organelles, especially mitochondria.

Oleate (OA) inhibits mitochondrial oxidative phosphorylation in PLIN2 null cells

The observation that interaction between LDs and mitochondria was dramatically increased in PLIN2 KO cells (Fig. 5A) raised the question whether the function of mitochondria would be affected. To answer this question, mitochondrial function was directly assessed by measuring cellular respiration in the EV and PLIN2 KO cells treated with or without OA. The oxygen consumption rate (OCR) (Fig. 6A) and linked ATP production (Fig. 6B) were decreased significantly in PLIN2 KO cells compared to the EV cells after treatment with OA. Even though the basal OCR did not change much (Fig. 6C), both the maximal OCR and the spare respiration capacity of PLIN2 KO cells were significantly inhibited after OA treatment (Fig. 6D and E). Taken together, these data suggest a dramatic decrease in mitochondrial respiration activity, especially after OA treatment, when PLIN2 is disrupted.

Previously, we found that cold treatment of mice could induce TAG hydrolysis, accompanied with closer interactions between LDs and mitochondria in brown adipose tissue (Yu *et al.* 2015). Thus, the accelerated TAG hydrolysis in PLIN2 null LDs (Fig. 3D, E) might activate mitochondria, inducing close interaction between LDs and mitochondria. To examine this, EV and

PLIN2 KO C2C12 cells were treated with or without lipases inhibitors (Atglistatin for the inhibition of ATGL, CAY10499 for the inhibition of HSL), and OA plus trace amount ^{3}H-OA for 12 h. The LDs were then isolated as previously described and LD proteins were extracted for silver staining and Western blot detection (supplementary material Fig. S6). The association of mitochondrial proteins (Cpt1a, Cpt1b, Opa1, and Mfn1) with LDs was not blocked by lipase inhibition; rather a slight increase was seen (supplementary material Fig. S6). Therefore, the interaction between LDs and mitochondria may be independent of accelerated TAG hydrolysis in PLIN2 KO cells.

DISCUSSION

In this study, we show that OA induced the expression of PLIN2 and the formation of LDs. Disruption of LDs reduces the stability of PLIN2 during OA treatment despite the increased PLIN2 transcriptional level. Depletion of PLIN2 enhances LD size and lipolysis activity, which indicates that PLIN2 and LDs reciprocally stabilize each other. In addition, our results also suggest that PLIN2 null LDs have weaker organelle compartmentalization as PLIN2 null LDs show enhanced interactions with the other cellular organelles, especially mitochondria. The increased interaction of LDs and mitochondria may contribute to inhibition of mitochondrial oxidative phosphorylation in PLIN2 KO cells during OA treatment. These results suggest that PLIN2 and LDs reciprocally stabilize each other and PLIN2 helps alleviate mitochondrial stress during OA treatment.

The data described herein bring us a step closer to a more complete understanding of PLIN2 function on LDs. PLIN2 is known to be abundantly expressed in skeletal muscle (Bosma *et al.* 2012; Brasaemle *et al.* 1997; Heid *et al.* 1998; MacPherson and Peters 2015b; Minnaard *et al.* 2009; Peters *et al.* 2012). We found that PLIN2 was the most abundant protein in the proteome of LDs isolated from the mouse myoblast cell line C2C12 and that, as expected, PLIN2 null LDs lack this abundant band by silver staining (supplementary material Fig. S3). The abundance of PLIN2 on LDs of C2C12 cells increased during OA treatment (Fig. 1B). The increased abundance of PLIN2 on LDs of OA-treated C2C12 cells plays an important role for the stability of the expanded LDs (Thiam *et al.* 2013).

Treatment with OA dramatically increases the mRNA and protein levels of PLIN2 in C2C12 cells, which is consistent with the previous reports (Bosma *et al.* 2012; de Wilde *et al.* 2010). Furthermore, the increase of PLIN2 protein was dramatically higher than its mRNA,
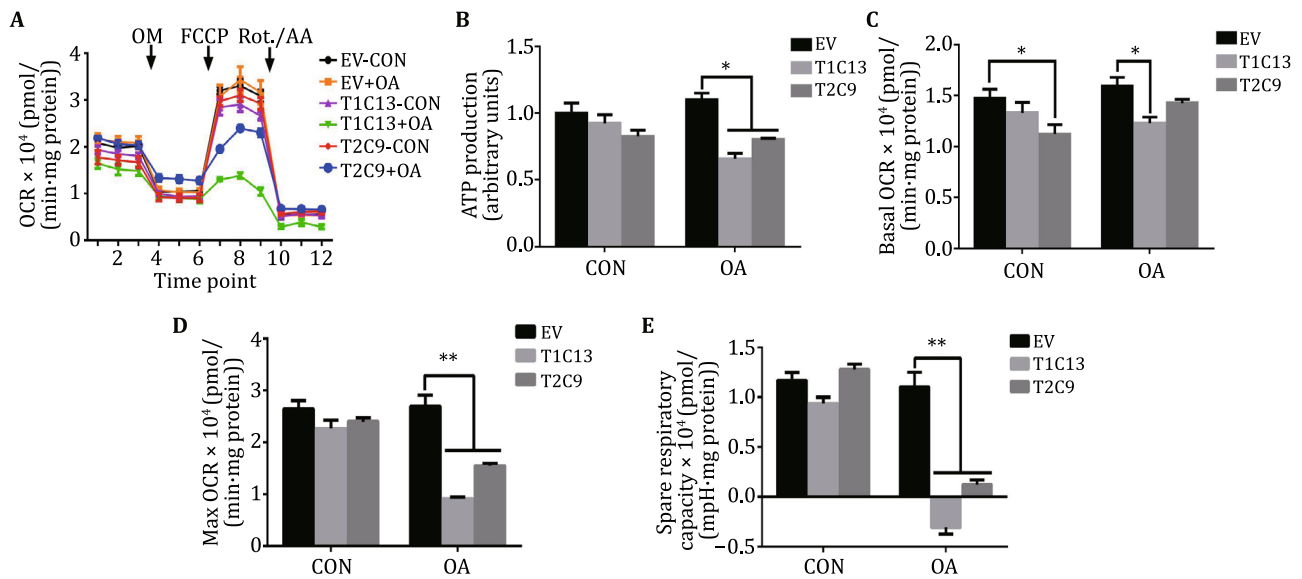
Fig. 6 OA inhibits mitochondrial oxidative phosphorylation in PLIN2 null cells. **A** OCR of EV and PLIN2 KO C2C12 cells after treatment with or without OA for 12 h. **B–E** The related ATP production (**B**), basal OCR (**C**), max OCR (**D**), and spare respiration capacity (**E**) are shown, respectively. Data are presented as mean ± SEM, and from two biological repeats. Significant difference between two groups, *$p < 0.05$, **$p < 0.01$

indicating that PLIN2 possessed posttranslational modification to regulate its stability under OA treatment. As shown in previous reports, the proteasome degradation pathway (Masuda *et al.* 2006; Takahashi *et al.* 2016; Xu *et al.* 2005) and chaperone mediated autophagy (Kaushik and Cuervo 2015, 2016) may play roles in the stability of PLIN2.

OA also drove the accumulation of TAG and the formation of LDs. However, it was unclear whether the PLIN2 expression increased LD number or if LD formation stabilized PLIN2 resulting in PLIN2 accumulation (MacPherson and Peters 2015a). Our data highlight that the formation of LDs is probably a prerequisite for the stability of PLIN2 (Fig. 2). When the formation of LDs was disrupted through a DKO of *Dgat1/Dgat2*, the accumulation of PLIN2 protein in response to OA treatment was blocked (Fig. 2D). However, the PLIN2 mRNA expression was still up-regulated (Fig. 2C).

PLIN2 null mice have been reported to be resistant to high fat diet-induced obesity and fatty liver disease (Chang *et al.* 2006; Libby *et al.* 2016; McManaman *et al.* 2013). Consistently, we demonstrated that PLIN2 KO C2C12 cells accumulated much less TAG than WT cells after OA treatment (Fig. 3C). However, the accumulation rate of TAG showed no difference between WT cells and PLIN2 KO cells (Fig. 3E). This may be explained if PLIN2 inhibits hydrolysis of TAG in LDs (Bell *et al.* 2008;

Listenberger *et al.* 2007), but has no effect on the rate of TAG synthesis.

Consistent with the reports by Bell *et al.* (2008) in mouse liver and Bosma *et al.* (2012) in skeletal muscle, the PLIN2 KO cells had fewer but larger LDs than WT cells (Fig. 4). PLIN2 was dramatically up-regulated on LDs of C2C12 cells during OA treatment (Fig. 1B), an increase which might serve to stabilize the organelle during LD expansion. We speculate that the enlarged LDs in PLIN2 KO cells might due to increased LD fusion activity in PLIN2 KO cells, but this requires further investigation. On the other hand, studies of subcellular localization of LDs indicate that PLIN2-enriched domains in the ER membrane might be involved in budding of LDs from the ER (Robenek *et al.* 2006). It is possible that PLIN2 KO cells display fewer LDs due to decreased budding events. Distinguishing between these hypotheses and elucidating the molecular mechanisms will require further work.

ATGL was reduced on PLIN2 null LDs (Fig. 3F), which was unexpected given the high lipolysis activity of PLIN2 null LDs in this study. This result was also inconsistent with previous reports that PLIN2 overexpression induced a striking decrease in the association of ATGL with LDs in HEK 293 cells (Listenberger *et al.* 2007) and the finding that PLIN2 down-regulation induced an increase in the association of ATGL with LDs

(Bell *et al.* 2008; Kaushik and Cuervo 2015). One possible explanation is that PLIN2 interacts with ATGL on LDs to maintain basal lipolysis (MacPherson *et al.* 2013) and most of PLIN2 associated ATGL was released to cytoplasm in PLIN2 KO cells. The elevated lipolysis activity of PLIN2 null LDs might be due to the re-localization and activation of HSL on LDs (Fig. 3F) and the full activation of the remaining LD-associated ATGL. How ATGL affects PLIN2 null LDs lipolysis remains to be defined.

LDs have been reported to interact with many other intracellular organelles (Goodman 2008; Murphy *et al.* 2009). Our data provide original insight into the important role of PLIN2 in the compartmentalization of LDs. We found that the association of marker proteins of some membrane structures, including ER, plasma membrane, lysosome, and mitochondria, was significantly increased in PLIN2 null LDs (Fig. 5A), suggesting enhanced interaction between LDs and the other intracellular organelles in PLIN2 KO cells. LDs have been found to physically interact with mitochondria (Nan *et al.* 2006; Pu *et al.* 2011; Sturmey *et al.* 2006), and the contact is further strengthened during exercise (Koves *et al.* 2013; Tarnopolsky *et al.* 2007). In this study, we found that deletion of PLIN2 dramatically increased the interaction between LDs and mitochondria as well as other organelles (Fig. 5A). Furthermore, both TEM and fluorescence imaging of whole cells and isolated LDs consistently showed an increased close interaction between LDs and mitochondria when PLIN2 was deleted (Fig. 5C–F). Thus, as the most abundant LD coat protein in C2C12 cells, PLIN2 may have a pivotal role in regulating the interaction between LDs and mitochondria.

Our previous work demonstrated that the expression and LD localization of PLIN2 are up-regulated in mouse brown adipose tissue during cold treatment, accompanied with increased interaction between LDs and activated mitochondria (Yu *et al.* 2015). It has been observed previously that the close physical interaction between LDs and mitochondria is positively correlated with the expression of PLIN2 and the activity of mitochondria (Yu *et al.* 2015). On the contrary, our data here indicate that the physical interaction between LDs and mitochondria was induced in PLIN2 null C2C12 cells, accompanied by a suppression of mitochondrial activity, especially during OA treatment (Fig. 6). Thus, the interaction was negatively correlated with the expression of PLIN2 and the activity of mitochondria. Notably, both studies show that PLIN2 expression is positively correlated with mitochondrial activation. These data indicate that the role of PLIN2 may be tissue specific (MacPherson and Peters 2015a).

MATERIALS AND METHODS

Cell culture

Mouse C2C12 myoblasts (American Type Culture Collections, Manassas, VA) were maintained in DMEM (Macgene Biotech., Beijing) supplemented with 10% FBS (Hyclone), 100 U/mL penicillin and 100 mg/mL streptomycin (Macgene Biotech., Beijing) at 37 °C, 5% CO_2.

Lipid droplets (LDs) isolation and verification

LDs were isolated using methods previously described with modification (Zhang *et al.* 2011). Briefly, $1-5 \times 10^9$ C2C12 myoblasts were collected with ice-cold PBS, and were transferred to 50 mL buffer A (20 mmol/L tricine pH 7.8, 250 mmol/L sucrose) plus 0.5 mmol/L PMSF (Sigma-Aldrich). After centrifugation at 3000 *g*, cell pellets were resuspended with 20 mL buffer A plus 0.5 mmol/L PMSF and kept on ice for 20 min. Then, the swollen cells were homogenized by nitrogen cavitation (500 psi for 15 min on ice). The PNS, Cyto, TM, and LD fractions were separated by centrifugation following procedures described previously (Zhang *et al.* 2011). The purified LDs were stained with LTR or LTG (1:500 (*v/v*), Life Technologies), and visualized using a ZEISS AxioImager M2 Imaging System or confocal microscope. The sizes of the purified LDs were measured by a Delsa Nano C particle analyzer as described previously (Zhang *et al.* 2012).

The lipids and the proteins of the LDs were extracted and separated with acetone before centrifuging the sample at 20,000 *g* for 10 min at 4 °C. The extracted proteins were dissolved in 2× sample buffer for biochemical analysis. The purity of LDs, relative to other cell fractions, was identified by silver staining and Western blotting for the LDs marker proteins described in our previous study (Bartz *et al.* 2007).

Fatty acids incubation

Sodium palmitic acid (Sigma-Aldrich) and sodium oleic acid were prepared as described previously (Peng *et al.* 2011). Briefly, fatty acids were mixed with ethanol to a final concentration of 100 mmol/L after which the mixture was sonicated on ice until the mixture became a milky solution. Before use, the fatty acids were dissolved in 55 °C preheated growth medium, and then cooled down to 37 °C. Cells were transferred to OA medium and cultured for the indicated period. Control cells were cultured in media containing an equivalent volume of ethanol as a vehicle control.

Quantitative real-time PCR

Total RNA was extracted with TRIzol reagent and reverse transcribed into cDNA according to the manufacturer's protocol (Life Technologies). Quantitative real-time PCR was performed using the ABI Step One PLUS and SYBR Green detection kit following the manufacturer's instructions (Life Technologies).

Western blot analysis

Cells were harvested and directly lysed with $2\times$ sample buffer (125 mmol/L Tris Base, 20% glycerol, 4% SDS, 4% β-mercaptoethanol, and 0.04% bromophenol blue). After sonication and denaturation, the samples were cooled to room temperature (RT) and then were loaded on 10% SDS-PAGE gel, electrophoresed, transferred to a PVDF membrane (Sigma-Aldrich), and blocked in 5% non-fat milk for 1 h at RT. Then, the PVDF membrane was incubated with primary antibodies and then secondary antibodies. The membrane was exposed to the ECL substrate (PerkinElmer Life Sciences, Waltham, MA) as described previously (Yu *et al.* 2015). The antibodies used in this study are listed in supplementary material Table S3.

Construction of plasmids and cell transfection

The CRISPR/Cas9 system was used to knock out and knock in target genes in C2C12 cells. For PLIN2 KO cell lines, two targets corresponding separately to exon 4 and exon 5 of PLIN2 were designed using the website (http://crispr.mit.edu/) and were inserted into the pX260a plasmid (a gift from Prof. Feng Zhang (Cong *et al.* 2013)). For *Dgat1* and *Dgat2* KO cell lines, two targets corresponding to these two genes, respectively, were designed using the website (http://crispr.mit.edu/) and were inserted into the pX260a plasmid. The KO detection primers for these KO cells were designed as displayed in supplementary material Table S4. For PLIN2-EGFP KI cell lines, a target near the stop codon of PLIN2 was designed and was inserted into the pX260a plasmid. Two pairs of homologous arm primers were designed and inserted into the pKI-EGFP-N plasmid with *Xba* I and *Nt.Bbvc* I restriction endonucleases. The pKI-EGFP-N plasmid was modified from pTK-NEO-3flag-USER in John Wang's lab and the functional sequence of pKI-EGFP-N is displayed in supplementary material Fig. S1A. For the real-time PCR detection of target genes, primers were designed according to NCBI BLAST and displayed in supplementary material Table S4. All plasmids were sequenced right by Tsingke Technologies Inc.

For cell transfection, pQCXIP derived plasmids were packaged into pseudo retrovirus in Plat-ET cells, and the virus was used to infect target cells. In some instances, plasmids were transfected into C2C12 cells using electroporation according to the manufacturer's instructions (Amaxa Nucleofector).

Cell line construction

For stable overexpression cells, C2C12 cells were infected with pQCXIP-Atgl-myc or pQCXIP-Plin2-myc typed pseudo retrovirus. Cells were incubated with 1 μg/mL puromycin containing DMEM medium starting 48 h after infection and were cultured for at least two weeks. Cells were then seeded into 96-well plates with limiting dilution and were cultured for another two weeks before picking clones. The expression state of the clones was verified by Western blot.

For KO cells, C2C12 cells were transfected with a targeted KO plasmid. Cells were incubated with 1 μg/mL puromycin containing DMEM medium 48 h after transfection and were selected as previously described. The selected KO status of the clones was verified by Western blot and/or genome PCR. For KI cells, C2C12 cells were co-transfected with targeted KO plasmid and homologous arms plasmids. Cells were sorted by flow cytometry (BD Aria III) 48 h after transfection and were selected as previously described. The selected KI clones were confirmed by Western blot.

Confocal microscopy

Various cell types were treated with OA as indicated. Cells were fixed in 4% paraformaldehyde and the LDs and nucleus were stained with LTR and Hochest (Life Technologies), respectively, for 30 min. The coverslips were then mounted with antifade solution (Applygen Technologies Inc., Beijing) and were sealed with nail polish. Images were captured with an Olympus FV1000 fluorescence confocal microscope (Olympus Corp., Lake Success, NY).

Detection of TAG and lipids

For the TAG accumulation assay, the indicated cells were subcultured into 12-well plates. The cells were then treated with or without 200 μmol/L OA with or without 0.5 μCi/mL ³H-oleic acid (³H-OA) (PerkinElmer, Boston, MA) for the indicated time. Cells were then lysed to detect the total TAG level (Biosino Bio-Technology and Science Inc, Beijing) or ³H-OA incorporated TAG by scintillation counter (PerkinElmer, Boston, MA) following thin layer chromatography (TLC).

For the assay of TAG lipolysis, the EV and PLIN2 KO cells were subcultured into 12-well plates. The cells were then pre-treated with or without ATGL inhibitor Atglistatin (10 μmol/L, Sigma, St. Louis, MO) (Mayer *et al.* 2013) and HSL inhibitor CAY10499 (1 μmol/L, Cayman, Michigan) (Saltiel 2000) for 2 h. Then, the cells were treated with OA supplemented with 0.5 μCi/mL ^{3}H-OA, with or without lipase inhibitors for another 12 h. TAG was extracted, and ^{3}H-OA incorporated TAG was assessed with a scintillation counter following TLC.

For the TAG synthesis assay, WT and PLIN2 KO cells were subcultured into 12-well plates. The cells were then treated with ^{3}H-OA (0.5 μCi/mL) and 200 μmol/L OA with 10 μmol/L Atglistatin and 1 μmol/L CAY10499. Cells were collected at the indicated times. The ^{3}H-OA incorporated TAG was assessed with a scintillation counter following TLC.

In all experiments, cells were harvested in 0.3 mL 1% Triton X-100/PBS to determine ^{3}H-OA incorporated TAG, and to assess total protein content (Pierce BCA assay, Thermo Scientific, Rockford, IL). The lipid extracts were separated by TLC using heptane-diethyl-ether (60:40:1, *v/v/v*) as developing solvent. The content of lipids was normalized to total protein content.

Cellular bioenergetics

The cellular bioenergetics profile of C2C12 cells was assessed using the Seahorse XF24 Flux Analyzer (Seahorse Bioscience) as described (Meex *et al.* 2015). In brief, the indicated cells were seeded into a 24-well XF24 cell culture microplate (Seahorse Bioscience). Cells were washed and incubated in 525 μL of unbuffered DMEM (5 mmol/L glucose, 1 mmol/L pyruvate and 1 mmol/L glutamate pH 7.4), at 37 °C in a non-CO_2 incubator (1 h prior to bioenergetics assessment). Three basal OCR measurements were performed using the Seahorse analyzer, and measurements were repeated following injection of oligomycin (1 μmol/L), FCCP (0.5 μmol/L), and Rotenone/Antimycin A (0.5 μmol/L).

Colloidal blue staining and comparative mass spectrum (MS) analysis

LD proteins isolated from C2C12 cells were separated on a 10% SDS-PAGE gel and subjected to colloidal blue staining (Life Technologies). The indicated bands were cut into slices for MS analysis. In-gel digestion of each slice was performed as previously described (Ding *et al.* 2012). The digested peptides were then loaded onto a C18 trap column with an autosampler, eluted onto a C18 column (100 μm × 12 cm) packed with Sunchrom packing material (SP-120-3-ODS-A, 3 μm), and were then subjected to nano LC-LTQ MS/MS analysis.

All MS/MS data were searched against the mouse protein database from the NCBI using the SEQUEST program (Thermo, USA). BioWorks search parameters were set as follows. Enzyme: trypsin; precursor ion mass tolerance: 2.0 Da; fragment ion mass tolerance: 1.0 Da. The variable modification was set to oxidation of methionine. The fixed modification was set to carboxyamidomethylation of cysteine. The search results were filtered with Xcorr versus Charge values of Xcorr (+1) > 1.9, Xcorr (+2) > 2.5, and Xcorr (+3) > 3.75.

Transmission electron microscopy (TEM)

The ultra-structure of cells was examined by TEM through ultra-thin sectioning. After rinsing with 0.1 mol/L PB, the cells were fixed in 2% (*w/v*) glutaraldehyde (Electron Microscopy Sciences, Hatfield) in PB (pH 7.4) for 1 h and then collected to a 1.5 mL microcentrifuge tube. The cells were subsequently fixed in 1% (*w/v*) osmium tetroxide (Nakalai Tesque, Kyoto) with 1% potassium ferrocyanide (Sigma-Aldrich, Missouri) for 1.5 h at RT. After dehydration in an ascending concentration series of ethanol at RT, the cells were embedded in Embed 812 (Electron Microscopy Sciences, Hatfield) and were prepared as 70 nm sections using a Leica EM UC6 Ultramicrotome. After staining with 4% (*w/v*) uranyl acetate (Electron Microscopy Sciences, Hatfield) for 15 min and subsequently with lead citrate (Electron Microscopy Sciences, Hatfield) for 5 min at RT, the sections were viewed with a Tecnai Spirit electron microscope (FEI, Netherlands). Purified LDs were also examined by TEM through an ultra-thin sectioning method as described (Ding *et al.* 2013).

Statistical analyses

Data are presented as mean ± SEM unless specifically indicated. The statistical analyses were performed using GraphPad Prism 6 and Image J (NIH, USA). Comparison of significance between groups was performed using student *t*-tests.

Compliance with Ethical Standards

Animal Rights and Informed Consent This article does not contain any studies with human or animal subjects performed by any of the authors.

References

Bartz R, Zehmer JK, Zhu M, Chen Y, Serrero G, Zhao Y, Liu P (2007) Dynamic activity of lipid droplets: protein phosphorylation and GTP-mediated protein translocation. J Proteome Res 6:3256–3265

Bell M, Wang H, Chen H, McLenithan JC, Gong DW, Yang RZ, Yu D, Fried SK, Quon MJ, Londos C, Sztalryd C (2008) Consequences of lipid droplet coat protein downregulation in liver cells: abnormal lipid droplet metabolism and induction of insulin resistance. Diabetes 57:2037–2045

Bickel PE, Tansey JT, Welte MA (2009) PAT proteins, an ancient family of lipid droplet proteins that regulate cellular lipid stores. Biochem Biophys Acta 1791:419–440

Binns D, Januszewski T, Chen Y, Hill J, Markin VS, Zhao Y, Gilpin C, Chapman KD, Anderson RG, Goodman JM (2006) An intimate collaboration between peroxisomes and lipid bodies. J Cell Biol 173:719–731

Bosma M, Hesselink MK, Sparks LM, Timmers S, Ferraz MJ, Mattijssen F, van Beurden D, Schaart G, de Baets MH, Verheyen FK, Kersten S, Schrauwen P (2012) Perilipin 2 improves insulin sensitivity in skeletal muscle despite elevated intramuscular lipid levels. Diabetes 61:2679–2690

Brasaemle DL (2007) Thematic review series: adipocyte biology. The perilipin family of structural lipid droplet proteins: stabilization of lipid droplets and control of lipolysis. J Lipid Res 48:2547–2559

Brasaemle DL, Barber T, Wolins NE, Serrero G, Blanchette-Mackie EJ, Londos C (1997) Adipose differentiation-related protein is an ubiquitously expressed lipid storage droplet-associated protein. J Lipid Res 38:2249–2263

Brown DA (2001) Lipid droplets: proteins floating on a pool of fat. Curr Biol 11:R446–R449

Chang BH, Li L, Paul A, Taniguchi S, Nannegari V, Heird WC, Chan L (2006) Protection against fatty liver but normal adipogenesis in mice lacking adipose differentiation-related protein. Mol Cell Biol 26:1063–1076

Chang BH, Li L, Saha P, Chan L (2010) Absence of adipose differentiation related protein upregulates hepatic VLDL secretion, relieves hepatosteatosis, and improves whole body

insulin resistance in leptin-deficient mice. J Lipid Res 51:2132–2142

Coll T, Eyre E, Rodriguez-Calvo R, Palomer X, Sanchez RM, Merlos M, Laguna JC, Vazquez-Carrera M (2008) Oleate reverses palmitate-induced insulin resistance and inflammation in skeletal muscle cells. J Biol Chem 283:11107–11116

Cong L, Ran FA, Cox D, Lin S, Barretto R, Habib N, Hsu PD, Wu X, Jiang W, Marraffini LA, Zhang F (2013) Multiplex genome engineering using CRISPR/Cas systems. Science 339:819–823

de Wilde J, Smit E, Snepvangers FJ, de Wit NW, Mohren R, Hulshof MF, Mariman EC (2010) Adipophilin protein expression in muscle–a possible protective role against insulin resistance. FEBS J 277:761–773

Ding Y, Yang L, Zhang S, Wang Y, Du Y, Pu J, Peng G, Chen Y, Zhang H, Yu J, Hang H, Wu P, Yang F, Yang H, Steinbüchel A, Liu P (2012) Identification of the major functional proteins of prokaryotic lipid droplets. J Lipid Res 53:399–411

Ding Y, Zhang S, Yang L, Na H, Zhang P, Zhang H, Wang Y, Chen Y, Yu J, Huo C, Xu S, Garaiova M, Cong Y, Liu P (2013) Isolating lipid droplets from multiple species. Nat Protoc 8:43–51

Fujimoto T, Parton RG (2011) Not just fat: the structure and function of the lipid droplet. Cold Spring Harb Perspect Biol 3(3):a004838

Fukushima M, Enjoji M, Kohjima M, Sugimoto R, Ohta S, Kotoh K, Kuniyoshi M, Kobayashi K, Imamura M, Inoguchi T, Nakamuta M, Nawata H (2005) Adipose differentiation related protein induces lipid accumulation and lipid droplet formation in hepatic stellate cells. In Vitro Cell Dev Biol Anim 41:321–324

Gao D, Griffiths HR, Bailey CJ (2009) Oleate protects against palmitate-induced insulin resistance in L6 myotubes. Br J Nutr 102:1557–1563

Goodman JM (2008) The gregarious lipid droplet. J Biol Chem 283:28005–28009

Greenberg AS, Coleman RA, Kraemer FB, McManaman JL, Obin MS, Puri V, Yan QW, Miyoshi H, Mashek DG (2011) The role of lipid droplets in metabolic disease in rodents and humans. J Clin Investig 121:2102–2110

Heid HW, Moll R, Schwetlick I, Rackwitz HR, Keenan TW (1998) Adipophilin is a specific marker of lipid accumulation in diverse cell types and diseases. Cell Tissue Res 294:309–321

Kaushik S, Cuervo AM (2015) Degradation of lipid droplet-associated proteins by chaperone-mediated autophagy facilitates lipolysis. Nat Cell Biol 17:759–770

Kaushik S, Cuervo AM (2016) AMPK-dependent phosphorylation of lipid droplet protein PLIN2 triggers its degradation by CMA. Autophagy 12:432–438

Kelley DE, Goodpaster B, Wing RR, Simoneau JA (1999) Skeletal muscle fatty acid metabolism in association with insulin resistance, obesity, and weight loss. Am J Physiol 277:E1130–E1141

Kimmel AR, Brasaemle DL, McAndrews-Hill M, Sztalryd C, Londos C (2010) Adoption of PERILIPIN as a unifying nomenclature for the mammalian PAT-family of intracellular lipid storage droplet proteins. J Lipid Res 51:468–471

Koves TR, Sparks LM, Kovalik JP, Mosedale M, Arumugam R, DeBalsi KL, Everingham K, Thorne L, Phielix E, Meex RC, Kien CL, Hesselink MK, Schrauwen P, Muoio DM (2013) PPAR-gamma coactivator-1alpha contributes to exercise-induced regulation of intramuscular lipid droplet programming in mice and humans. J Lipid Res 54:522–534

Larigauderie G, Cuaz-Perolin C, Younes AB, Furman C, Lasselin C, Copin C, Jaye M, Fruchart JC, Rouis M (2006) Adipophilin increases triglyceride storage in human macrophages by stimulation of biosynthesis and inhibition of beta-oxidation. FEBS J 273:3498–3510

Libby AE, Bales ES, Orlicky DJ, McManaman JL (2016) Perilipin-2 deletion impairs hepatic lipid accumulation by interfering with SREBP activation and altering the hepatic lipidome. J Biol Chem 291(46):24231–24246

Listenberger LL, Ostermeyer-Fay AG, Goldberg EB, Brown WJ, Brown DA (2007) Adipocyte differentiation-related protein reduces the lipid droplet association of adipose triglyceride lipase and slows triacylglycerol turnover. J Lipid Res 48:2751–2761

Liu P, Ying Y, Zhao Y, Mundy DI, Zhu M, Anderson RG (2004) Chinese hamster ovary K2 cell lipid droplets appear to be metabolic organelles involved in membrane traffic. J Biol Chem 279:3787–3792

Liu P, Bartz R, Zehmer JK, Ying YS, Zhu M, Serrero G, Anderson RG (2007) Rab-regulated interaction of early endosomes with lipid droplets. Biochem Biophys Acta 1773:784–793

MacPherson RE, Peters SJ (2015a) Piecing together the puzzle of perilipin proteins and skeletal muscle lipolysis. Appl Physiol Nutr Metab 40(7):641–651

MacPherson REK, Peters SJ (2015b) Piecing together the puzzle of perilipin proteins and skeletal muscle lipolysis. Appl Physiol Nutr Metab 40:641–651

MacPherson RE, Herbst EA, Reynolds EJ, Vandenboom R, Roy BD, Peters SJ (2012) Subcellular localization of skeletal muscle lipid droplets and PLIN family proteins OXPAT and ADRP at rest and following contraction in rat soleus muscle. Am J Physiol Regul Integr Comp Physiol 302:R29–R36

MacPherson RE, Ramos SV, Vandenboom R, Roy BD, Peters SJ (2013) Skeletal muscle PLIN proteins, ATGL and CGI-58, interactions at rest and following stimulated contraction. Am J Physiol Regul Integr Comp Physiol 304:R644–R650

Masuda Y, Itabe H, Odaki M, Hama K, Fujimoto Y, Mori M, Sasabe N, Aoki J, Arai H, Takano T (2006) ADRP/adipophilin is degraded through the proteasome-dependent pathway during regression of lipid-storing cells. J Lipid Res 47:87–98

Mayer N, Schweiger M, Romauch M, Grabner GF, Eichmann TO, Fuchs E, Ivkovic J, Heier C, Mrak I, Lass A, Höfler G, Fledelius C, Zechner R, Zimmermann R, Breinbauer R (2013) Development of small-molecule inhibitors targeting adipose triglyceride lipase. Nat Chem Biol 9:785–787

McManaman JL, Bales ES, Orlicky DJ, Jackman M, MacLean PS, Cain S, Crunk AE, Mansur A, Graham CE, Bowman TA, Greenberg AS (2013) Perilipin-2-null mice are protected against diet-induced obesity, adipose inflammation, and fatty liver disease. J Lipid Res 54:1346–1359

Meex RC, Hoy AJ, Mason RM, Martin SD, McGee SL, Bruce CR, Watt MJ (2015) ATGL-mediated triglyceride turnover and the regulation of mitochondrial capacity in skeletal muscle. Am J Physiol Endocrinol Metab 308:E960–E970

Minnaard R, Schrauwen P, Schaart G, Jorgensen JA, Lenaers E, Mensink M, Hesselink MKC (2009) Adipocyte differentiation-related protein and OXPAT in rat and human skeletal muscle: involvement in lipid accumulation and type 2 diabetes mellitus. J Clin Endocr Metab 94:4077–4085

Murphy S, Martin S, Parton RG (2009) Lipid droplet-organelle interactions; sharing the fats. Biochem Biophys Acta 1791:441–447

Nan X, Potma EO, Xie XS (2006) Nonperturbative chemical imaging of organelle transport in living cells with coherent anti-stokes Raman scattering microscopy. Biophys J 91:728–735

Ozeki S, Cheng J, Tauchi-Sato K, Hatano N, Taniguchi H, Fujimoto T (2005) Rab18 localizes to lipid droplets and induces their close apposition to the endoplasmic reticulum-derived membrane. J Cell Sci 118:2601–2611

Pan DA, Lillioja S, Kriketos AD, Milner MR, Baur LA, Bogardus C, Jenkins AB, Storlien LH (1997) Skeletal muscle triglyceride levels are inversely related to insulin action. Diabetes 46:983–988

Peng G, Li L, Liu Y, Pu J, Zhang S, Yu J, Zhao J, Liu P (2011) Oleate blocks palmitate-induced abnormal lipid distribution, endoplasmic reticulum expansion and stress, and insulin resistance in skeletal muscle. Endocrinology 152:2206–2218

Peters SJ, Samjoo IA, Devries MC, Stevic I, Robertshaw HA, Tarnopolsky MA (2012) Perilipin family (PLIN) proteins in human skeletal muscle: the effect of sex, obesity, and endurance training. Appl Physiol Nutr Me 37:724–735

Prats C, Donsmark M, Qvortrup K, Londos C, Sztalryd C, Holm C, Galbo H, Ploug T (2006) Decrease in intramuscular lipid droplets and translocation of HSL in response to muscle contraction and epinephrine. J Lipid Res 47:2392–2399

Pu J, Ha CW, Zhang S, Jung JP, Huh WK, Liu P (2011) Interactomic study on interaction between lipid droplets and mitochondria. Protein Cell 2:487–496

Robenek H, Hofnagel O, Buers I, Robenek MJ, Troyer D, Severs NJ (2006) Adipophilin-enriched domains in the ER membrane are sites of lipid droplet biogenesis. J Cell Sci 119:4215–4224

Russell TD, Palmer CA, Orlicky DJ, Bales ES, Chang BH, Chan L, McManaman JL (2008) Mammary glands of adipophilin-null mice produce an amino-terminally truncated form of adipophilin that mediates milk lipid droplet formation and secretion. J Lipid Res 49:206–216

Saltiel AR (2000) Another hormone-sensitive triglyceride lipase in fat cells? Proc Natl Acad Sci USA 97:535–537

Salvado L, Coll T, Gomez-Foix AM, Salmeron E, Barroso E, Palomer X, Vazquez-Carrera M (2013) Oleate prevents saturated-fatty-acid-induced ER stress, inflammation and insulin resistance in skeletal muscle cells through an AMPK-dependent mechanism. Diabetologia 56:1372–1382

Schrader M (2001) Tubulo-reticular clusters of peroxisomes in living COS-7 cells: dynamic behavior and association with lipid droplets. J Histochem Cytochem 49:1421–1429

Shaw C, Sherlock M, Stewart P, Wagenmakers A (2009) Adipophilin distribution and colocalisation with lipid droplets in skeletal muscle. Histochem Cell Biol 131:575–581

Sturmey RG, O'Toole PJ, Leese HJ (2006) Fluorescence resonance energy transfer analysis of mitochondrial: lipid association in the porcine oocyte. Reproduction 132:829–837

Takahashi Y, Shinoda A, Kamada H, Shimizu M, Inoue J, Sato R (2016) Perilipin2 plays a positive role in adipocytes during lipolysis by escaping proteasomal degradation. Sci Rep 6:20975

Tarnopolsky MA, Rennie CD, Robertshaw HA, Fedak-Tarnopolsky SN, Devries MC, Hamadeh MJ (2007) Influence of endurance exercise training and sex on intramyocellular lipid and mitochondrial ultrastructure, substrate use, and mitochondrial enzyme activity. Am J Physiol Regul Integr Comp Physiol 292:R1271–R1278

Thiam AR, Farese RV Jr, Walther TC (2013) The biophysics and cell biology of lipid droplets. Nat Rev Mol Cell Biol 14:775–786

Unger RH, Clark GO, Scherer PE, Orci L (2010) Lipid homeostasis, lipotoxicity and the metabolic syndrome. Biochem Biophys Acta 1801:209–214

Villena JA, Roy S, Sarkadi-Nagy E, Kim KH, Sul HS (2004) Desnutrin, an adipocyte gene encoding a novel patatin domain-containing protein, is induced by fasting and glucocorticoids. J Biol Chem 279:47066–47075

Walther TC, Farese RV Jr (2012) Lipid droplets and cellular lipid metabolism. Annu Rev Biochem 81:687–714

Xu G, Sztalryd C, Lu X, Tansey JT, Gan J, Dorward H, Kimmel AR, Londos C (2005) Post-translational regulation of adipose

differentiation-related protein by the ubiquitin/proteasome pathway. J Biol Chem 280:42841–42847

Yen CL, Stone SJ, Koliwad S, Harris C, Farese RV Jr (2008) Thematic review series: glycerolipids. DGAT enzymes and triacylglycerol biosynthesis. J Lipid Res 49:2283–2301

Yu J, Zhang S, Cui L, Wang W, Na H, Zhu X, Li L, Xu G, Yang F, Christian M, Liu P (2015) Lipid droplet remodeling and interaction with mitochondria in mouse brown adipose tissue during cold treatment. Biochem Biophys Acta 1853:918–928

Zhang H, Wang Y, Li J, Yu J, Pu J, Li L, Zhang H, Zhang S, Peng G, Yang F, Liu P (2011) Proteome of skeletal muscle lipid droplet reveals association with mitochondria and apolipoprotein a-I. J Proteome Res 10:4757–4768

Zhang P, Na H, Liu Z, Zhang S, Xue P, Chen Y, Pu J, Peng G, Huang X, Yang F, Xie Z, Xu T, Xu P, Ou G, Zhang SO, Liu P (2012) Proteomic study and marker protein identification of *Caenorhabditis elegans* lipid droplets. Mol Cell Proteomics 11:317–328

Zimmermann R, Strauss JG, Haemmerle G, Schoiswohl G, Birner-Gruenberger R, Riederer M, Lass A, Neuberger G, Eisenhaber F, Hermetter A, Zechner R (2004) Fat mobilization in adipose tissue is promoted by adipose triglyceride lipase. Science 306:1383–1386

Zimmermann R, Lass A, Haemmerle G, Zechner R (2009) Fate of fat: the role of adipose triglyceride lipase in lipolysis. Biochim Biophys Acta 1791:494–500